As_{2}Te_{3} glass under high hydrostatic pressure: Polyamorphism, relaxation, and metallization

V. V. Brazhkin, E. Bychkov, and O. B. Tsiok

Phys. Rev. B **95**, 054205 — Published 22 February 2017

DOI: 10.1103/PhysRevB.95.054205

As_2Te_3 glass under high hydrostatic pressures: Polyamorphism, relaxation and metallization

V. V. Brazhkin[1*], E. Bychkov[2] and O. B. Tsiok[1]

[1]*Institute for High Pressure Physics, Russian Academy of Sciences, Troitsk, Moscow, 108840 Russia*

[2]*LPCA, UMR 8101 CNRS, Universite du Littoral, 59140 Dunkerque, France*

Abstract

High-precision measurements of the specific volume and electrical resistivity of As_2Te_3 glasses are performed under hydrostatic pressures up to 8.5 GPa. A smooth transformation and logarithmic relaxation of the density is observed at pressures higher than 1 GPa. The softening of the effective bulk modulus and the relaxation rate have a sharp maximum at 2.5 GPa, which is indicative of the existence of polyamorphism. At pressures above 4.5 GPa, a new relaxation process begins. During decompression, the pressure dependence of the compressibility exhibits a kink near 4 GPa. The electrical resistivity decreases by almost eight orders of magnitude, most sharply in the range of 2–3.5 GPa (by three orders of magnitude). Smooth metallization occurs at a pressure of 5 GPa; the resistivity decreases to a value of $1.7 \cdot 10^{-4}$ Ω cm at 8.1 GPa. Under decompression, the electrical resistivity exhibits a hysteresis and returns to values three orders of magnitude smaller than the initial one. The volume and electrical resistivity under normal conditions relax to quasi-equilibrium values in several months. The relaxed glasses with a smaller chemical disorder have a lower electrical resistivity. The results together with the data on the structure and dynamics in As_2Te_3 glasses allow conclusions on the mechanism of pressure-induced transformations.

Introduction

Tellurium-based chalcogenide glasses are technologically important substances that have found wide applications in phase change memory and infrared photonics [1]. Of particular interest are the As_xTe_{100-x} glasses that serve as model systems, but an atomistic understanding of the structure−property relations in it remains obscure due to controversies [2-15]. The As_2Te_3 melt, similar to the Te melt, is a metal at small overheating above the melting temperature [16,17], as a result, cooling-induced crystallization can be avoided only at quenching rates above 100 K/s. The structure of As_2Te_3 glasses is previously considered as similar to the structure of a classical network (As_2S_3-type) based on corner-sharing trigonal $AsTe_{3/2}$ pyramids [2]. However, it was established more recently that stoichiometric glassy *g*-As_2Te_3 strongly differs in structure of the short-range order from the crystalline phase and is characterized by a chemical disorder of 30 to 60% (chemical disorder is defined as the number of homopolar As-As bonds to the total number of As-Te and As-As bonds) [3-12]. Furthermore, the analysis of the structure of *g*-As_2Te_3 is also complicated because of a strong dependence on the fabrication procedure [8,15]. Unfortunately, any adequate model of the structure of the short- and intermediate-range orders for *g*-As_2Te_3 glasses is still absent.

As_2Te_3 glasses have a small semiconducting gap (≈0.8 eV); for this reason, these glasses are very attractive for the study of the pressure-induced metallization. *g*-As_2Te_3 glass is the only stoichiometric chalcogenide glass that is metallized at pressures below 10 GPa [18], and it can be studied in bulk samples under pure hydrostatic conditions. At the same time, studies of *g*-As_2Te_3 under pressure are scarce. The metallization of *g*-As_2Te_3 was observed at pressures ≈10 GPa and was accompanied in some studies by crystallization [19], whereas metallization of amorphous sputtered films *a*-As_2Te_3 in [20] occurred with the conservation of the amorphous state. The superconductivity of the metallic state also has been studied [21]. The electrical resistivity of the bulk glasses *g*-As_2Te_3 was studied at a pressure up to 6.5 GPa [22]. All studies of the electrical resistivity of compressed *a*-As_2Te_3 and *g*-As_2Te_3 were performed under nonhydrostatic conditions excluding moderate pressures up to 1 GPa [23]. It is interesting that *g*-As_2Te_3 is an example of a few glasses whose vitrification and crystallization temperatures decrease rapidly (at a rate of 2−3 K/kbar) with an increase in the pressure [24]. The structure and other characteristics of *g*-As_2Te_3 glasses under pressure, including such a fundamental characteristic as compressibility, have not been studied at all. Since the structure of *g*-As_2Te_3 glasses strongly differs from the simple network, an anomalous behavior of the compressibility and other characteristics under pressure can be expected.

The aim of this work is a high-precision study of the compressibility, relaxation processes, and electrical resistivity of *g*-As_2Te_3 glasses at high pressures up to 8.5 GPa under pure hydrostatic conditions.

Experimental Methods

Initial glasses were obtained from pure elementary substances As (99.9999%) and Te (99.997%) (Aldrich Chemical Ltd.). To fabricate the glass the pristine As_2Te_3 substances were placed in preliminarily cleaned quartz tubes with an inner diameter of 8 mm, which were then evacuated and pressurized. Melts were aged and mixed for 6 h at 600ºC and, after that, were annealed in water. The initial ingots had pores with sizes of several tens of microns, which prevent measurements without additional measures because cracks appeared in the samples even at pressures of 0.7–1.2 GPa. Thus, glass samples needed an additional treatment both for the "healing" of pores and for the removal of chemical order inhomogeneities. A strong dependence of the structure and degree of chemical order on the quenching temperature in glassy arsenic telluride is also well known. A feature of As_2Te_3 stoichiometric glass is an increased tendency to crystallization. It appeared that both softening and crystallization of this glass occur in a very narrow temperature range: softening begins at 130−135ºC and crystallization begins at ~ 145ºC (at a heating rate of ~ 1 K/min). The experimentally chosen regime of thermobaric treatment (hot pressing) with the parameters of 0.2 GPa, 136ºC, and 3 min allowed obtaining pore-free samples without a noticeable impurity of a crystalline phase. The required accuracy of maintenance of the parameters of the hot-pressing process appeared to be very high: when the temperature of treatment was increased by 2ºC, about 0.5−1% of the crystalline phase appeared in the sample.

Neutron diffraction experiments were carried out using the SANDALS diffractometer at the ISIS spallation neutron source (Rutherford-Appleton Laboratory, U.K.). Low-energy Te resonances are limited the available range of the scattering vector $Q = 4\pi \sin\theta/\lambda$ to 25 $Å^{-1}$, where 2θ is the scattering angle and λ the neutron wavelength). The neutron diffraction data were corrected for background and container scattering, self-attenuation, multiple scattering, and inelasticity (Placzek) effects to obtain the total neutron structure factor $S_N(Q)$.

High-energy X-ray diffraction experiments were conducted at the 6-ID-D beamline at APS (Argonne National Laboratory, USA). The X-ray energy was 100.329 keV, providing data at Q values up to 30 $Å^{-1}$. A 2D setup was used for data collection with a PerkinElmer model 1621 X-ray area detector. The two-dimensional diffraction patterns were reduced using the Fit2D software. The measured background intensity was subtracted, and corrections were made for the different detector geometries and efficiencies, sample self-attenuation, and Compton scattering using standard procedures giving the total X-ray structure factor $S_X(Q)$.

The resulting glass samples had a density of 5.55 g/cm^3 and were free of pores and impurity of the crystalline phase (see Fig.1). The compressibility and electrical resistivity were measured for 3×2×1.5- and 2.5×1×0.7-mm rectangular samples, respectively. After high pressure study all samples were preserved in a glassy state (see Fig.1).

High-pressure experiments were performed in a Toroid apparatus [25]. The volume of amorphous samples under hydrostatic pressure was measured at room temperature (294K) by the strain gauge method [26]. This method was successfully applied to study both oxide and chalcogenide glasses (see, e.g., [27,28]).The absolute error of measuring the volume in this method is 0.15% and the sensitivity of measurements is 10^{-5}. A methanol–ethanol (4:1) mixture with a hydrostatic limit of about 10 GPa was used as a pressure-transmitting medium. The pressure was measured by a calibrated manganin gauge. The reproducibility of the pressure scale was better than 0.01 GPa.

The volume was measured under the continuous variation of the pressure at a rate of 0.08–0.12 and 0.03–0.05 GPa/min with increasing and decreasing pressure, respectively. When studying the kinetics of densification of glasses at a fixed pressure, the pressure was maintained with an accuracy of 2 MPa.

The electrical resistivity of the glasses was measured by the four-probe method. We experimentally selected a low-temperature solder, three-component eutectic In–Bi–Sn (3:1:1 atomic). The possible error of data on the absolute value of the electrical resistivity is determined by errors of determination of the geometric factor of the samples and was estimated as 7-10%.

Results

The pressure dependences of the volume of *g*-As_2Te_3 for three different samples are shown in Fig. 2. Both at an increase and a decrease in the pressure, measurements were performed with a small pressure step of 0.02GPa; for this reason, the resulting curve is almost continuous and does not require interpolation. It is seen that the compression curves are not approximated by a single simple equation of state and the elastic behavior is observed only up to a pressure of 1 GPa. The bulk modulus in the initial segment of compression is $B = (15.85 \pm 0.1)$ GPa and its derivative is $dB/dP = 6.1 \pm 0.1$. The volume decreases anomalously in the pressure range of 2–3.5 GPa and an additional increase in the density in this transformation is about 2.5%. Pressure hysteresis between the curves at increasing and decreasing pressures is small and the residual densification is about 2%; in this case, the volume under normal conditions relaxes to the initial value in several months. A logarithmic time dependence (relaxation) of the volume of *g*-As_2Te_3 glass samples at a fixed pressure is observed at pressures above 1 GPa (Fig. 3). Deviation from the logarithmic dependence at small times is due to a finite rate of the pressure increase in the

experiment. The relaxation rate has a sharp maximum at 2.5 GPa (see the inset of Fig. 3); in this case, the relaxation rate is close to the maximum values for $GeSe_2$ glasses, for which a transition to a flexible network is observed in a narrow pressure range [28].

The effective bulk moduli of glasses was obtained by direct differentiation over points without additional processing. Figure 4 shows the effective bulk moduli for *g*-As_2Te_3 glasses as functions of the pressure and density. A linear increase in the bulk modulus with the pressure is observed up to 1 GPa; with a further increase in the pressure, the derivative dB/dP decreases and becomes negative (the bulk modulus is softened). This is accompanied by intense volume relaxation, which continues up to the highest pressures, and the bulk modulus obtained by differentiation corresponds to the effective relaxing values. The difference between the relaxing and relaxed bulk moduli indicates the existence of activation processes and smooth transformations in glasses [27-29]. The maximum softening of the relaxing bulk modulus is observed at 2.5 GPa coinciding with the pressure at which the relaxation rate is maximal. After long-term isobaric relaxations, the effective bulk modulus at a further increase in the pressure first corresponds to high relaxed values and then decreases to effective relaxing values corresponding to a curve with a constant loading rate («forgets» its prehistory) (see Fig. 4). Small irregularities in the relaxing bulk modulus reproduce variations of the rate of the pressure in a region where relaxation occurs. At pressures above 4.5 GPa, the slope of the pressure dependence of the effective bulk modulus decreases also apparently because of the gradual adding of new relaxation processes.

After decompression, glasses behave elastically up to 1.5 GPa and the bulk modulus corresponds to relaxed values. At lower pressures, a more intense decrease in the effective bulk modulus begins because of relaxation processes in the reverse transformation. It is interesting that the pressure dependence of the bulk modulus at decreasing pressure exhibits a kink at 4 GPa, where the derivative dB/dP decreases from 8 to 5.5. The bulk moduli of *g*-As_2Te_3 glasses at decreasing pressure are close to those after isobaric relaxations at the increasing-pressure stage (see Fig. 4), which likely indicates that the structure of the short-range order in these glasses is the same at increasing and decreasing pressure [28]. It is interesting that the density dependences of the effective bulk moduli at increasing and decreasing pressure are joined in the density range of 6.55–6.7 g/cm^3 (see the lower plot in Fig. 4).

Figure 5 shows the pressure dependences of the electrical resistivity of the glasses for both «fresh» glass samples after quenching from a melt and samples relaxed after hot pressing. The initial resistivity of relaxed glasses $(1.1-1.2)\cdot10^3$ Ω cm) is an order of magnitude lower than that of quenched glasses ($(0.83-0.95)\cdot10^4$ Ω cm). For comparison, the figure shows early data for amorphous films *a*-As_2Te_3 and *g*-As_2Te_3 bulk glasses obtained under nonhydrostatic conditions [20,22]. It is seen that previous rough measurements were performed with a large error,

particularly at pressures $P > 2$ GPa. The electrical resistivity of glasses decreases exponentially with an increase in the pressure to 1.5−2 GPa; after that, an anomalously fast decrease in the electrical resistivity by almost three orders of magnitude is observed in the narrow pressure range of 2−3.5 GPa, where the largest changes in the volume (by 5.8%) were also observed. At pressures above 3 GPa, the pressure dependences of the electrical resistivity for different types of glasses are almost joined in one; i.e., a glass «forgets» the features of the initial state. Since the characteristic values of the minimum metallic conductivity for chalcogenide glasses are $(1–4)\cdot10^{-3}$ Ω cm [30], it can be concluded that a transition to a metallic state occurs at pressures of 4−5 GPa. Metallization proceeds smoothly without crystallization. With a further compression, the resistivity continues to slowly decrease, reaching $1.7\cdot10^{-4}$ Ω cm at 8.1 GPa. One can note the resistivity of the metallic melt varies from $3\ 10^{-2}$ to $6\ 10^{-4}$ Ω cm [16]. The time logarithmic relaxation of the resistivity is observed up to maximum pressures as for the volume (see the inset of Fig. 5). The reverse metal–insulator transition at decompression occurs at 2.5–3.5 GPa. After decompression, the electrical resistivity of the samples was two and three orders of magnitude (!) lower than the initial value for the hot pressed and quenched samples, respectively, although the residual densification was as small as 2% (Fig. 5). A long-term aging under normal conditions results in an increase in the resistivity to values characteristic of hot pressed samples. The time dependences of the volume and resistivity of samples under normal conditions are shown in Fig. 6. It is interesting that the rate of resistivity change with the volume at increasing and decreasing pressure is much lower than that at isobaric relaxation (see Fig. 7). A decrease in the resistivity when the volume changes by 1% is only 25% (instead of 100% for isobaric aging) at the maximum pressures and is 70−120% (instead of 570% for relaxation at atmospheric pressure) at the minimum pressures.

Discussion and Conclusions

The results allow a number of conclusions on the features of the behavior of *g*-As_2Te_3 glasses under pressure and on their metallization. First, glasses can be classified into three groups depending on prehistory: (i) first type - freshly prepared glasses after quenching from the melt, (ii) second type - relaxed glasses obtained by hot pressing, and (iii) third type - glasses after hydrostatic compression up to 8.5 GPa and subsequent relaxation. The analysis of the structural data (see Fig. 8 and corresponding Table 1) shows that the minimum and maximum chemical disorders are inherent in the samples of the third and first types, respectively. At first glance, this is counterintuitive because metallization under pressure usually reduces the degree of covalence and increases chemical disorder. However, at the same time, a fast decrease in the vitrification and crystallization temperature with an increase in the pressure should significantly accelerate local diffusion under compression. It can be assumed that the «healing» of defects and chemical

disorder occurs at pressures of 2.5−3.5 GPa even more intensively than at the annealing of glasses at low pressures. Another counterintuitive fact is that samples with smaller chemical disorder have a lower electrical resistivity (see Fig. 9). We suppose that a large number of wrong neighbors and defects lead to a high degree of localization of carriers and to an increase in the gap in mobility in spite of a formally higher «metallicity» (the number of Te−Te neighbors).

The sharp softening of the effective bulk modulus of *g*-As_2Te_3 at pressures of 2−2.5 GPa is quite similar to the behavior of $GeSe_2$ glasses [28]. It can be assumed that local elastic constants for structural units, which are $AsTe_{3/2}$ pyramids joined along the edges (tetrahedra for $GeSe_2$), are softened as for $GeSe_2$ glasses. One can suppose that the amorphous network for *g*-As_2Te_3 is built on both corner- and edge-sharing $AsTe_{3/2}$ pyramids (see Fig. 10). Intense relaxation processes in *g*-As_2Te_3 at pressures of 2−3 GPa are likely due to a change in the type of connectivity of pyramids from a «common edge» to a «common corner» similar to g-$GeSe_2$. The sharpest decrease in the electrical resistivity by three orders of magnitude under variation of pressure from 2 to 3.5 GPa begins at the same pressures. At the same time, there are significant differences in behavior of these two glasses. The softening of bulk moduli of $GeSe_2$ in the range of 2–3 GPa occur in the elastic regime and intense relaxation processes begin only at a further increase in the pressure [28]. Relaxation processes and softening of the effective bulk modulus in As_2Te_3 glasses begin simultaneously at pressures above 1 GPa. It can be assumed that inelastic chemical ordering processes are imposed on the processes of softening of the bulk modulus and the subsequent change in the intermediate-range order.

Because of a low vitrification temperature and a high mobility of atoms, the samples at pressures of 3−3.5 GPa «forget» their prehistory and the electrical resistivities of different initial samples approach a common dependence. The metallization of As_2Te_3 glasses occurs at pressures of 4−5 GPa, which is half of the previously accepted value. At pressures above 4.5 GPa, the smooth variation of the intermediate order possibly occurs without a significant change in coordination and chemical ordering possibly continues with easier diffusion in the metallic state. A possible error in preceding measurements of the electrical resistivity in [20,22] was due to nonhydrostatic conditions and poor measuring contacts; furthermore, amorphous films rather than bulk glasses were studied in [20]. The absolutely smooth pressure dependence of the electrical resistivity in the wide pressure range of 5−8.5 GPa indicates that As_2Te_3 glasses in the metallic state are not crystallized.

An interesting effect detected in this work is a kink on the pressure dependence of the bulk modulus near 4 GPa at a decrease in the pressure. Any noticeable structural transformations and relaxations are absent in this pressure range at decreasing pressure. This behavior is possibly attributed to a significant contribution from conduction electrons to the bulk modulus and its

derivative in the metal region. The residual densification (≈2%) and anomalously low electrical resistivity (~ 10 Ω cm) immediately after decompression are apparently due to the partial irreversibility of a change in the type of connectivity of $AsTe_{3/2}$ pyramids. The amorphous network relaxes to a quasi-equilibrium state at long-term aging (for 10^7 s) under normal conditions. An anomalously high rate of the resistivity variation with the volume at isobaric relaxation (see Fig. 6) indicates that relaxation processes without changing the volume affect the resistivity.

In summary, we revealed the main characteristics of transformations in *g*-As_2Te_3 glasses under pressure. The elastic behavior is observed up to 1 GPa; a polyamorphic transformation without changing the coordination number, which is accompanied by a strong softening of the effective bulk modulus and the intensive logarithmic relaxation of the density, occurs from 1.5 to 3 GPa; an inelastic behavior with weak relaxation associated with chemical ordering is observed in the range of 4.5–8.5 GPa; and smooth metallization occurs at 4−5 GPa. The transformation in the glasses is almost completely reversible. Subsequent detailed structural studies of polyamorphism and metallization in *g*-As_2Te_3 glasses under pressure, as well as ab initio computer simulations, are desirable. However, as was mentioned above, the data on the short- and intermediate-range orders in As_2Te_3 glasses even at normal pressure are contradictory. We hope that this work will stimulate detailed experimental and theoretical studies of the structure and dynamics of As_2Te_3 glasses at normal and high pressures.

Acknowledgments

We are grateful to N.F. Borovikov and I.P. Zibrov for assistance in the chemical and phase analysis of samples. The authors also thank Dr. C. J. Benmore for the help with high-energy X-ray diffraction measurements. Work at the Advanced Photon Source, Argonne National Laboratory, was supported in part by the Office of Basic Energy Sciences, U. S. Department of Energy, under Contract No. DE-AC02-06CH1135. This work was supported by the Russian Science Foundation (project no. 14-22-00093).

Reference List

[1] M. Wuttig and N. Yamada, Nat. Mater. **6**, 824 (2007).

[2] J. Cornet and D. Rossier J. Non-Cryst. Sol. **12**, 85 (1973).

[3] Q. Ma, D. Raoux and S. Benazeth, Phys. Rev. B **48**, 16332 (1993).

[4] K. Abe, O. Uemura, T. Usuki, Y. Kameda and M. Sakurai, J. Non-Cryst. Solids **232-234**, 682 (1998).

[5] H. Endo, H. Hoshino, H. Ikemoto and T. Miyanaga, J. Phys. Condens. Matter **12**, 6077 (2000).

[6] P. Jóvári, S. N. Yannopoulos, I. Kaban, A. Kalampounias, I. Lishchynskyy, B. Beuneu, O. Kostadinova, E. Welter and A. Schöps, J. Chem. Phys. **129**, 214502 (2008).

[7] S. Sen, S. Joshi, B.G. Aitken, and S. Khalid, J. Non-Cryst. Solids **354**, 4620 (2008).

[8] A. Tverjanovich, K. Rodionov, and E. Bychkov, J. Solid-State Chem. **190**, 271 (2012).

[9] D. C. Kaseman, I. Hung, K. Lee, K. Kovnir, Z. Gan, B. Aitken, and S. Sen, J. Phys. Chem. B **119**, 2081 (2015).

[10] M. Dongol, T. Gerber, M. Hafiz, M. Abou-Zied, and A.F. Elhady, J. Phys.: Condens. Matter, **18**, 6213 (2006).

[11] T.G. Edwards, E.L. Gjersing, S. Sen, S.C. Currie, and B.G. Aitken, J. Non-Cryst. Solids **357**, 3036 (2011).

[12] M. Tenhover, P. Boolchand, and W.J. Bresser, Phys. Rev. B **27**, 7533 (1983).

[13] S. S. K. Titus, R. Chatterjee, S. Asokan, and A. Kumar, Phys. Rev. B **48**, 14650 (1993).

[14] S. Sen, S. Soyer Uzun, C.J. Benmore, and B.J. Aitken, J. Phys.: Condens. Matter **22**, 405401 (2010).

[15] A. Tverjanovich, M. Yagodkina, and V. Strykanov, J. Non-Cryst. Solids **223**, 86 (1998).

[16] H. Endo, H. Hoshino, H. Ikemoto, T. Miyanaga, J. Phys.: Condens. Matter **12**, 6077 (2000).

[17] C. Otjacques, J. Raty, F. Hippert, H. Schober, M. Johnson, R. Céolin, and J. Gaspard, Phys Rev. B **82**, 054202 (2010).

[18] G. Parthasarathy and E.S.R. Gopal, Bull. Mat. Sci. (1985) **7**, 271.

[19] S. Minomura, in: Amorphous semiconductors-Technologies and devices, ed. by Y. Hamakawa, Amsterdam: North Holland, 1978, p.245.

[20] N. Sakai and H. Fritzsche, Phys. Rev. B **15**, 973 (1977).

[21] I. V. Berman, N. V. Brandt, I. E. Kostyleva, S. K. Pavlov, V. I.Sidorov, and S. M. Chudinov, JETP Lett. **43**, 62 (1986).

[22] G. Ramani, A. Giridhar, and A.K. Singh, Phil. Mag. B **39**, 385 (1979).

[23] J. Kristofic, J.J. Mares, and V. Smid, Phys. Stat. Sol(a) **89**, 333 (1985).

[24] K. Ramesh, J. Phys. Chem. B **118**, 8848 (2014).

[25] L.G. Khvostantsev, V.N. Slesarev, and V.V. Brazhkin, High Press. Res. **24**, 371 (2004).

[26] O.B. Tsiok, V.V. Bredikhin, V.A. Sidorov, and L.G. Khvostantsev, High Pressure Research **10**, 523 (1992).

[27] O.B. Tsiok, V.V. Brazhkin, A.G. Lyapin, and L.G. Khvostantsev, Phys. Rev. Lett. **80**, 999 (1998).

[28] V.V. Brazhkin, E. Bychkov, and O.B. Tsiok, Phys. Chem. B **120**, 358 (2016).

[29] V.V. Brazhkin, O.B. Tsiok, and Y. Katayama, JETP Lett. **89**, 244 (2009) [Pis'ma v Zhetp. **89**, 285 (2009)].

[30] V.V. Struzhkin, A.F. Goncharov, R. Caracas, H.-k. Mao, and R.J. Hemley, Phys. Rev. B **77**, 165133 (2008).

Table 1. Structural parameters (nearest-neighbor distances and partial coordination numbers) of glassy As_2Te_3 before (A) and after thermal (B) and high-pressure treatment (C).

Sample	As-As		As-Te		Te-Te		$N_{Te-(As,Te)}$	Chemical disorder
	r (Å)	N_{As-As}	r (Å)	N_{As-Te}	r (Å)	N_{Te-Te}		
A	2.41	0.64	2.65	2.36	2.78	0.53	2.10	0.21
B	2.40	0.53	2.65	2.47	2.78	0.51	2.16	0.18
C	2.40	0.43	2.66	2.57	2.81	0.44	2.15	0.14

Chemical disorder is defined as the number of homopolar As-As bonds to the total number of As-Te and As-As bonds, $\frac{N_{As-As}}{N_{As-As}+N_{As-Te}}$.

The mean-square deviations (MSD) of the calculated parameters are ±0.01 Å for As-As and As-Te bond lengths, and ±0.02 Å for Te-Te distances. The MSD values for coordination numbers are ±0.02 for N_{As-As} and N_{As-Te}, and ±0.04 for N_{Te-Te}.

FIGURE CAPTIONS

Fig. 1. A low-Q part of the Faber-Ziman neutron $S_N(Q)$ (blue) and X-ray $S_X(Q)$ (green) structure factors of glassy g-As_2Te_3 plotted together with the diffraction pattern for the α-As_2Te_3 crystalline polymorph (red). The pulsed neutron data corresponds to freshly prepared g-As_2Te_3, the high-energy $S_X(Q)$ was obtained for g-As_2Te_3 recovered from 8.5 GPa.

Fig. 2. Pressure dependences of the volume of glassy As_2Te_3 at an increase (closed points) and a decrease (open points) in the pressure obtained in three experiments. In one of the experiments, the glass densification kinetics at pressure points marked by arrows was studied. The solid line is the approximation of the initial segments (0–1.2 GPa) of $V(P)$ dependences by the Murnaghan equation (B_0 = (15.85 ± 0.1) GPa and dB/dP = 6.1 ± 0.1). The inset shows a magnified image of the region near the maximum pressure, where densification kinetics was studied on one of the samples.

Fig. 3. Relaxation of the volume of glassy As_2Te_3 at a fixed pressure. Numbers near the curves are the exposure pressures in gigapascals. The inset shows the pressure dependence of the stationary relaxation rate determined as $-d(V/V_0)/d(\log t)$ in the linear segment of the time dependences.

Fig. 4. (a, upper and left scales) Apparent bulk moduli of glassy As_2Te_3 obtained from the initial $V(P)$ data by the formula $B = -VdP/dV$ at an increase (closed symbols) and a decrease (open symbols) in the pressure; the solid lines emphasize a kink on the pressure dependence of the bulk modulus at a decrease in the pressure. (b, lower and right scales) Same data for two experiments recalculated as functions of the density of samples; colors and symbols representing results of various experiments correspond to the notation in Fig. 1.

Fig. 5. Pressure dependences of the electrical resistivity of glassy As_2Te_3 at an increase (closed symbols) and a decrease (open symbols) in the pressure according to the results of two experiments (1 - «fresh» glass sample after quenching from a melt; 2 - sample relaxed after hot pressing) in comparison to the data from (triangles) [22] and (circles) [20] at an increase (filled symbols) and a decrease (open symbols) in the pressure. The inset shows the kinetics of variation of the electrical resistivity at the maximum pressure.

Fig.6. Relaxation of the (left scale, open symbols) volume and (right scale, closed symbols) electrical resistivity of glassy As_2Te_3 samples after decompression. Large symbols are measured electrical resistivities for two different samples remaining after the measurements of $V(P)$ and the volume relaxation.

Fig. 7. Derivative of the electrical resistivity of glassy As_2Te_3 versus the variation of the volume per 1% ΔV. The results of two experiments (Fig. 5) at (closed symbols) an increase and (open

symbols) a decrease in the pressure are recalculated using the $V(P)$ curves averaged over two experiments (Fig. 2) at an increase and a decrease in the pressure. The colors and symbols representing various experiments are the same as in Fig. 5. The points at the end of the dependence at decreasing pressure at ΔV smaller than 10% are smoothed. The volume dependence of the electrical resistivity cannot be correctly plotted in this region because of strong relaxations of both the volume and electrical resistivity. The values of the derivative at relaxations at the maximum pressure and after decompression, which were obtained as the ratios of steady relaxation rates of the electrical resistivity and volume, are also represented on the plot.

Fig. 8. (a) X-ray total correlation functions $T_X(r)$ for pristine *g*-As_2Te_3, glassy As_2Te_3 after heating to 130 °C, a temperature close to T_g,, and *g*-As_2Te_3 recovered from 8.5 GPa; a three-peak fitting of $T_X(r)$ for (b) the sample recovered from 8.5 GPa and (c) pristine glassy As_2Te_3. The first neighbour correlations are shown in red (As-As, ≈2.40Å), green (As-Te, ≈2.65 Å) and blue (Te-Te, ≈2.80 Å). The fitting parameters are shown in Table 1.

Fig. 9. Temperature dependencies of resistivity of glassy As_2Te_3 before (closed symbols) and after (open symbols) high pressure experiments. Only two of about 30 curves are shown for the relaxation behavior of resistivity after high pressure

Fig. 10. Hypothetical transformation of $(As_4Te_6)_n$ ribbon in crystalline α-As_2Te_3 into two chemically ordered motifs of *g*-As_2Te_3. (a) A single $(As_4Te_6)_n$ ribbon in the crystalline structure of monoclinic α-As_2Te_3 with octahedral As(2) and trigonal As(1) sites and a wide distribution of As-Te first neighbor distances, 2.82±0.11 Å. Since the As-Te interatomic distances in liquid and glassy As_2Te_3 are remarkably shorter, 2.65±0.03 Å, the network topology of α-As_2Te_3 will not survive on melting giving rise to alternative connectivity. (b) The bonding/non-bonding limit is set at 2.85Å. A single $(As_4Te_6)_n$ ribbon appears to be split into three chains: (i) the central string composed of edge-sharing pyramids, ES-$AsTe_{3/3}$, and (ii) two lateral chains consisting of corner-sharing units, CS-$AsTeTe_{2/2}$. The central string, ES-$AsTe_{3/3}$, loses every third As atom transforming (c) into a chain consisting of $AsTe_{3/2}$ pyramids with alternate edge- and corner-sharing, (d) the two lateral chains with remaining As species are forming a new As-Te ribbon consisting of As_3Te_3 and As_6Te_6 rings.

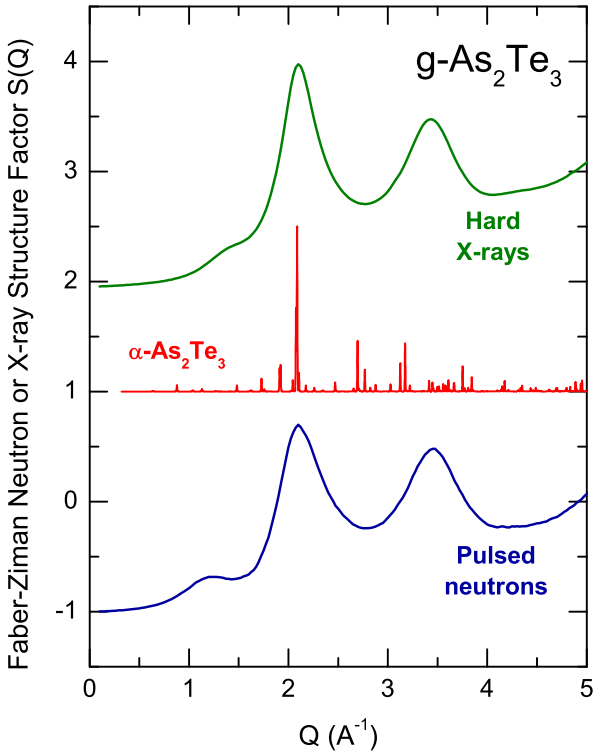

Figure 1 LY14978 30JAN2017

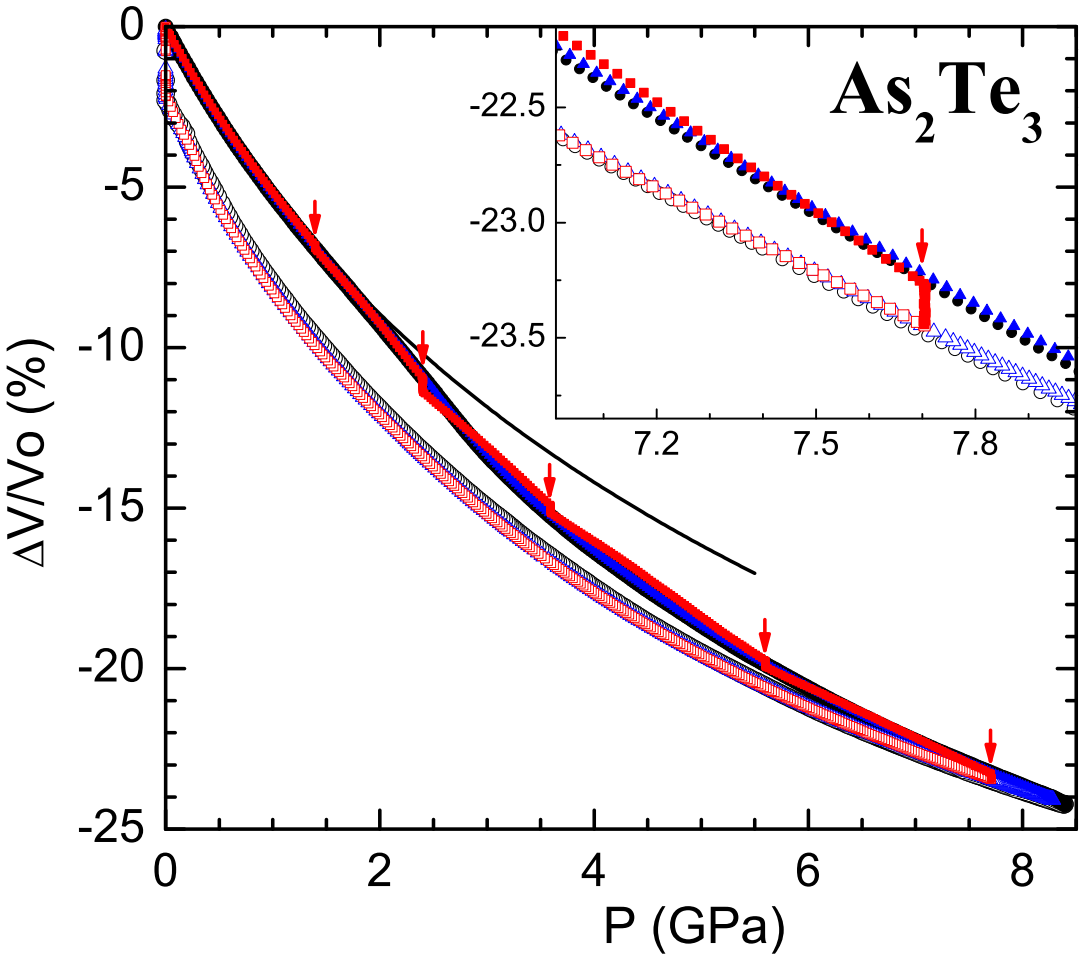

Figure 2 LY14978 30JAN2017

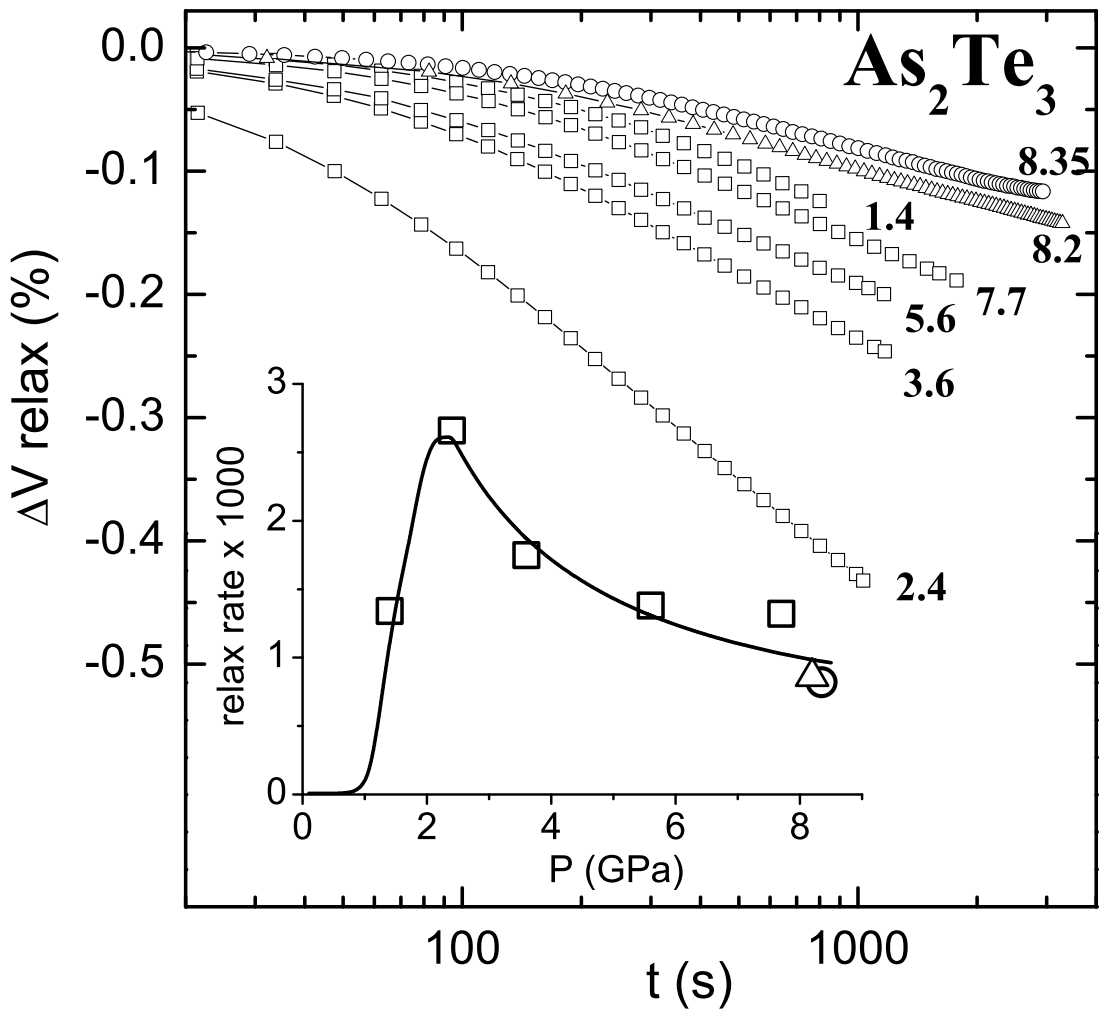

Figure 3 LY14978 30JAN2017

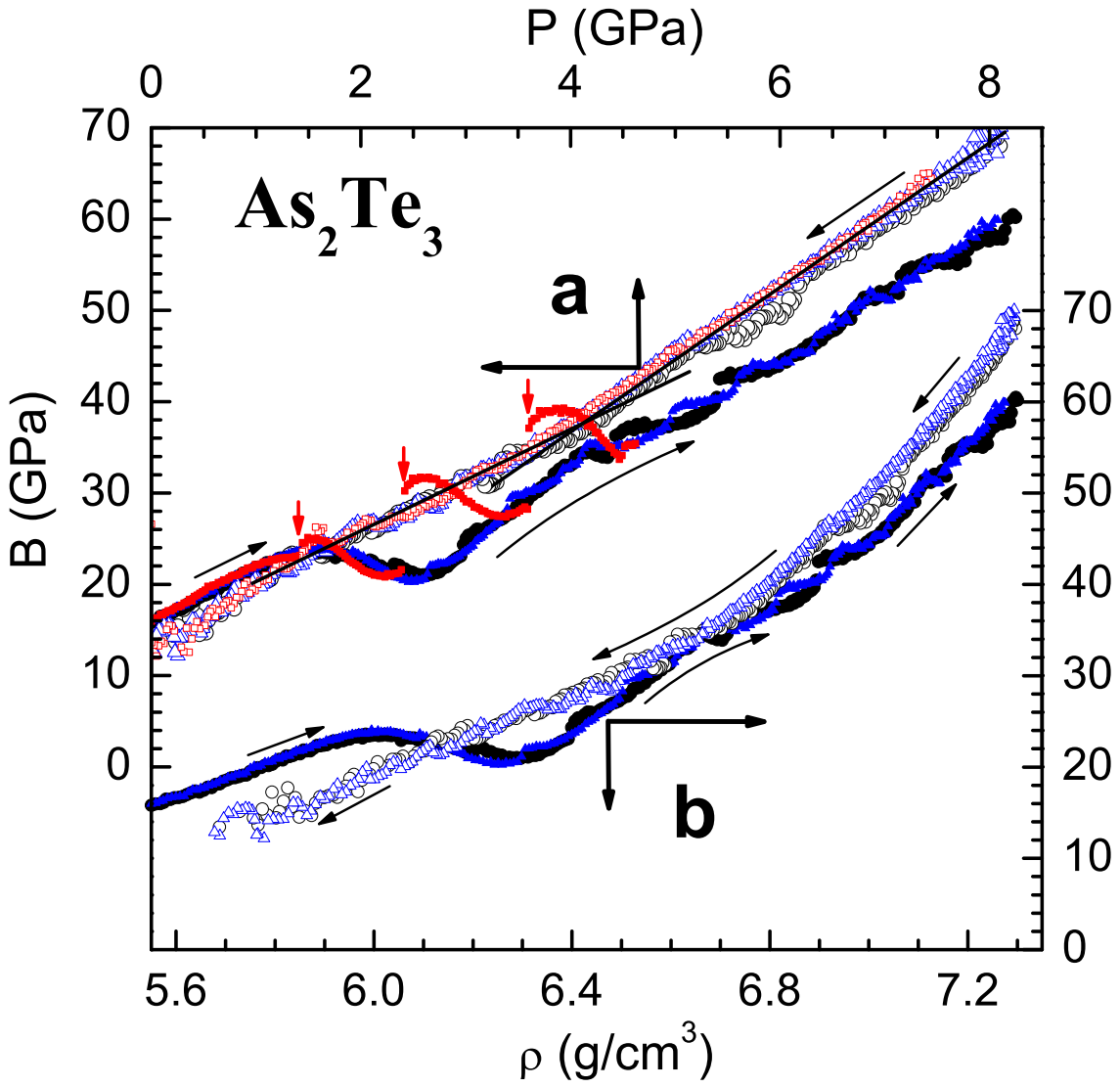

Figure 4 LY14978 30JAN2017

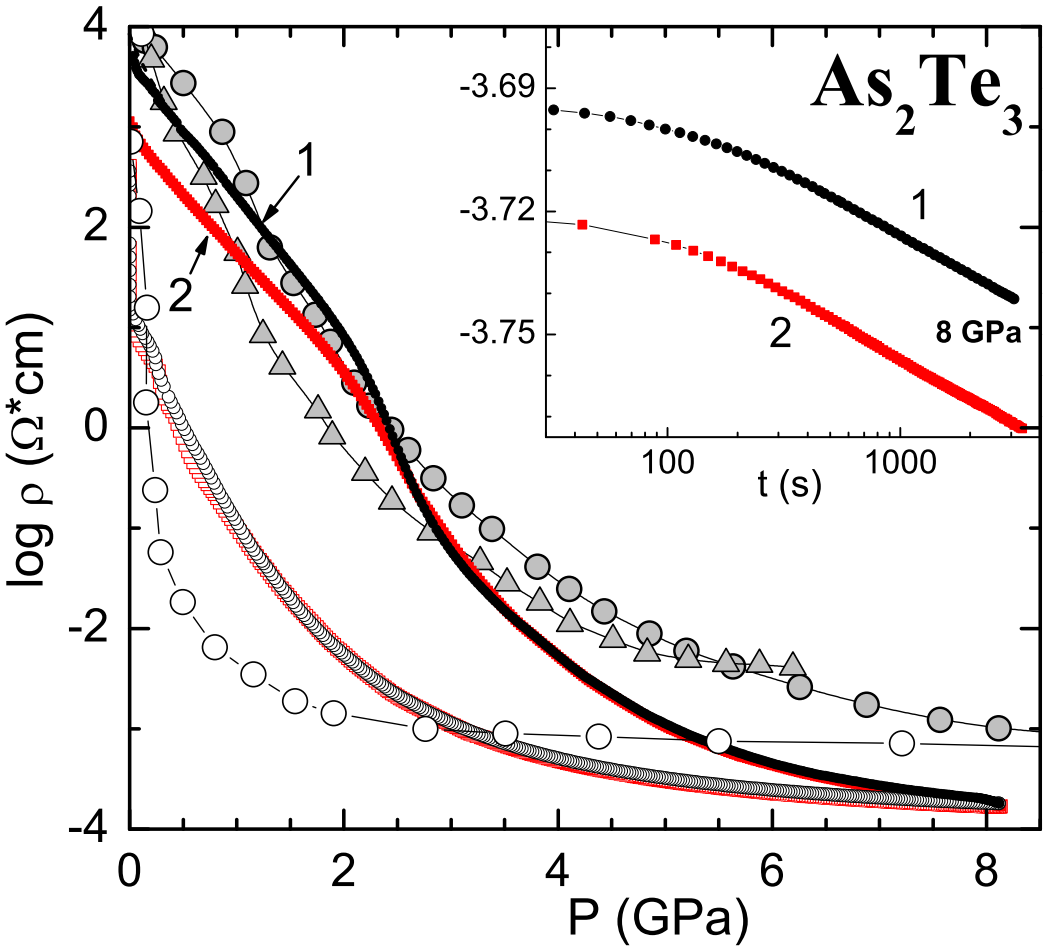

Figure 5 LY14978 30JAN2017

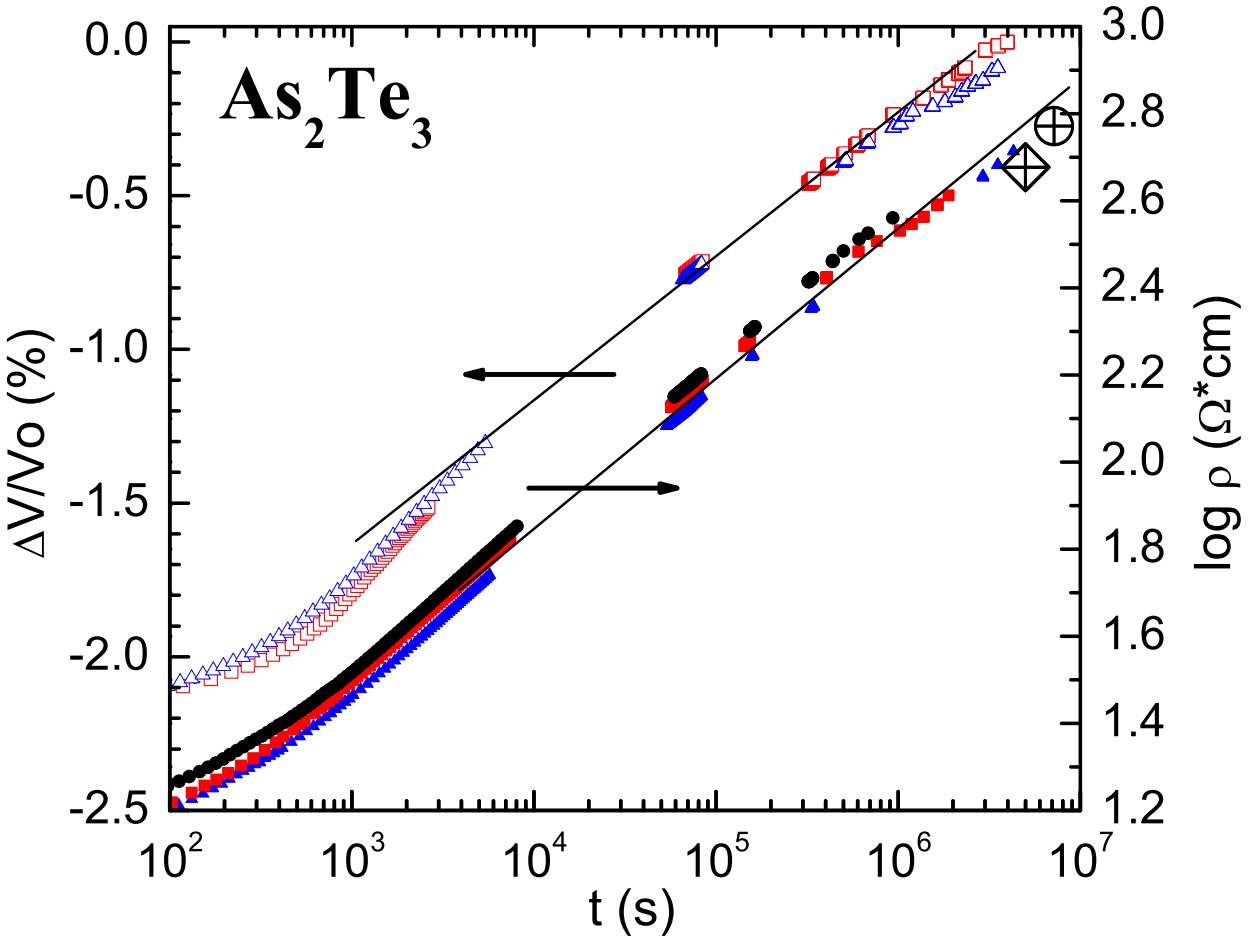

Figure 6 LY14978 30JAN2017

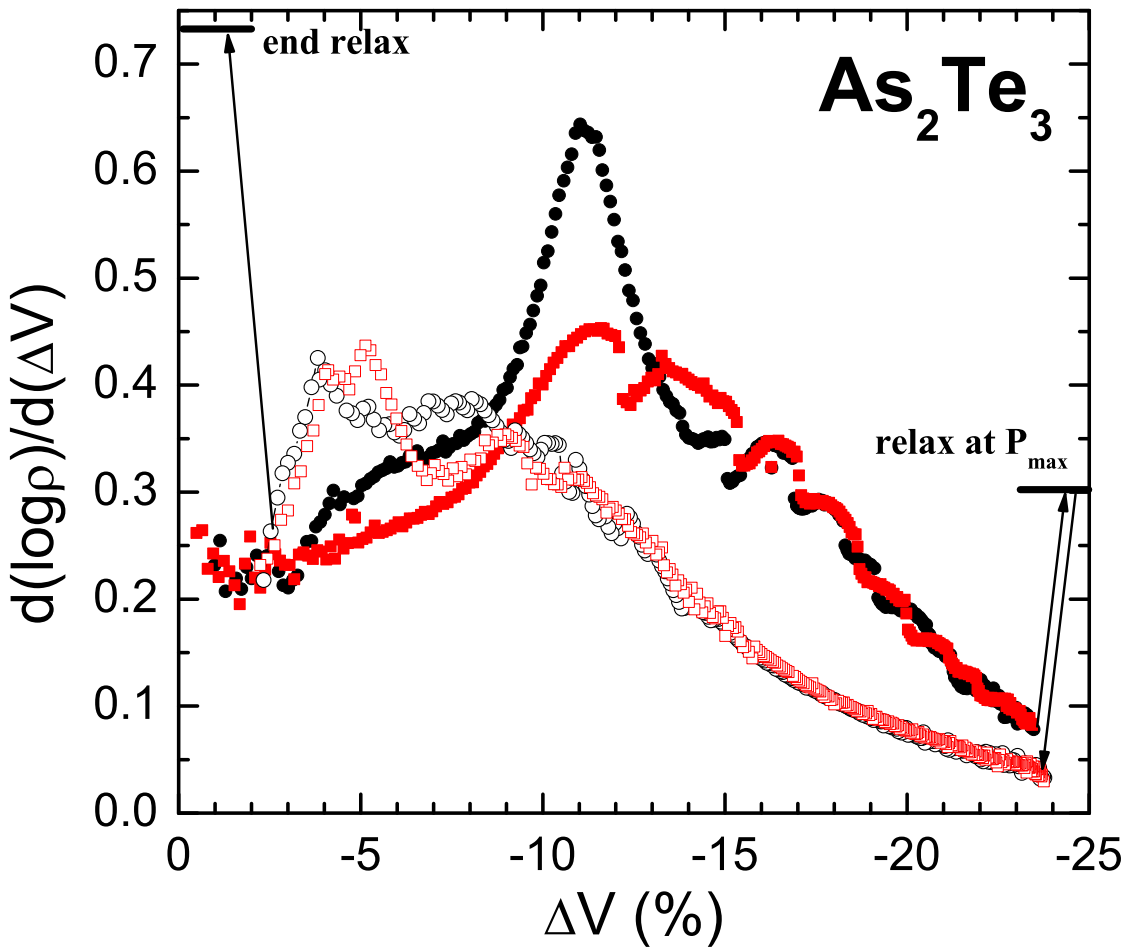

Figure 7 LY14978 30JAN2017

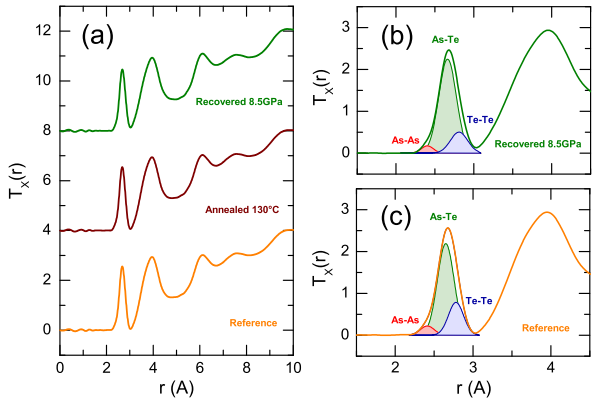

Figure 8 LY14978 30JAN2017

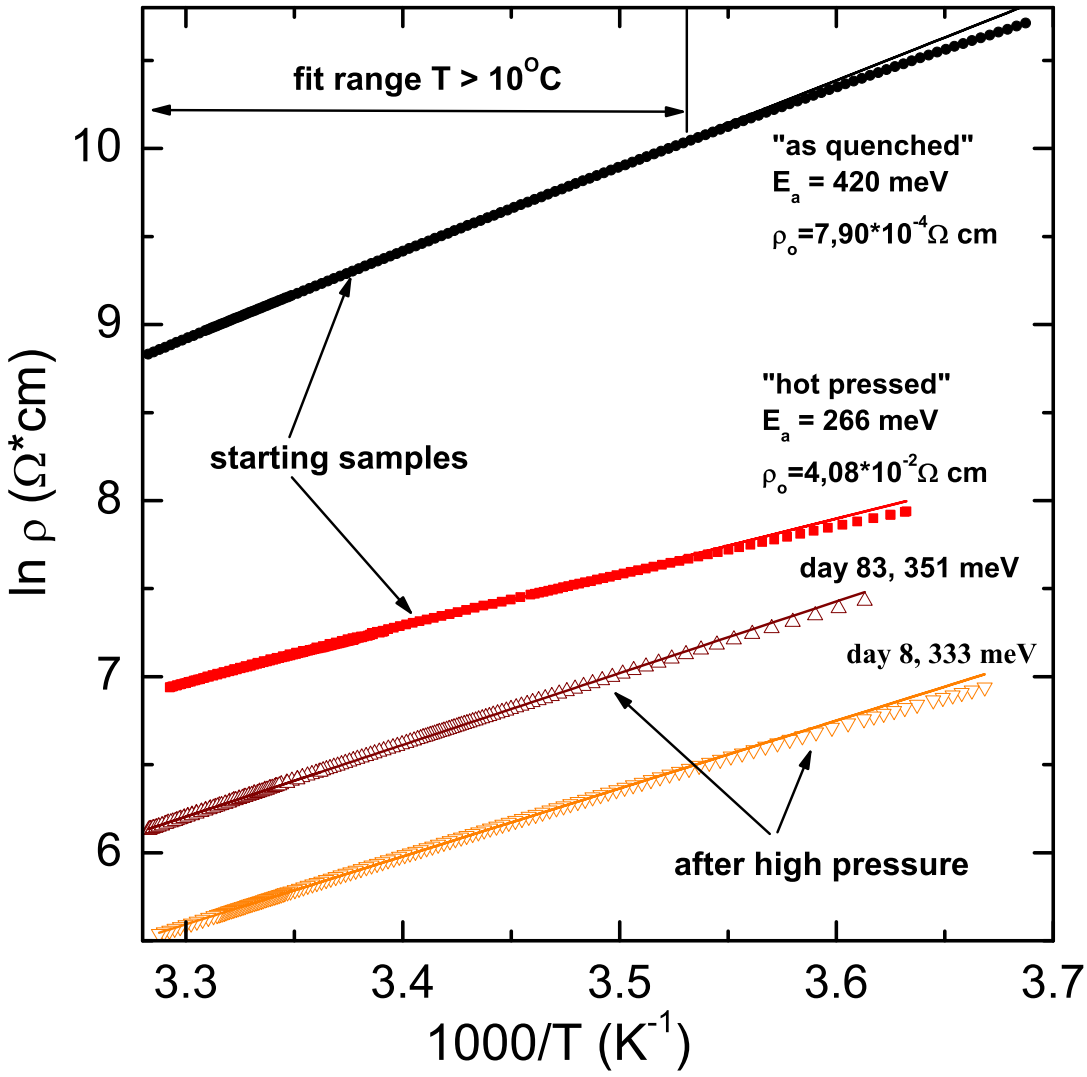

Figure 9 LY14978 30JAN2017

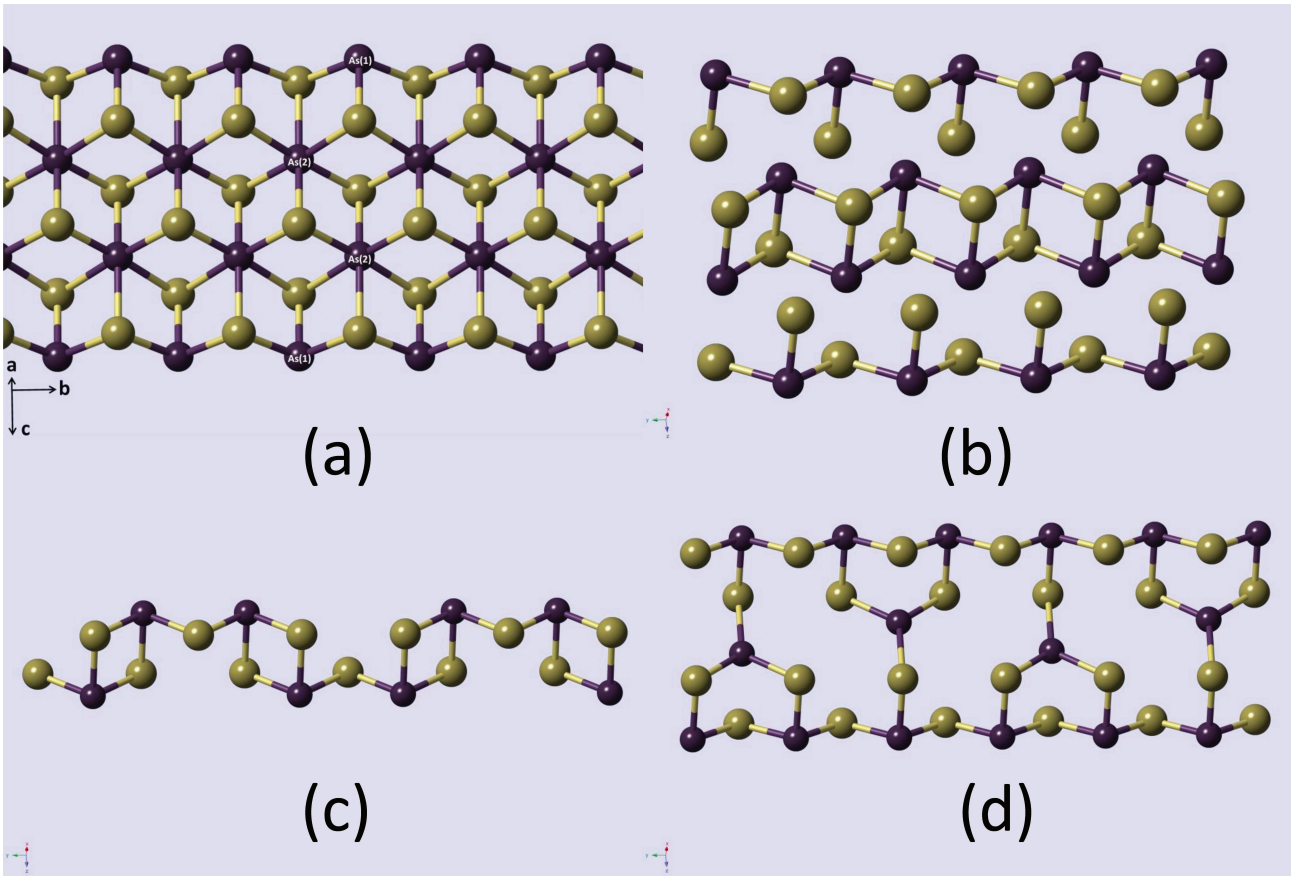

Figure 10 LY14978 30JAN2017